

Evolution of the pdf of a high Schmidt number passive scalar in a plane wake

H. Rehab, L. Djenidi and R. A. Antonia
Department of Mechanical Engineering
University of Newcastle, N.S.W. 2308 Australia

Key-words: passive scalar, mixing, probability density function, turbulent wake

ABSTRACT

Temporal statistics of the concentration fluctuation c of diluted fluorescein dye, a high Schmidt number passive scalar ($Sc = \nu/D \gg 2000$, ν and D are the fluid viscosity and scalar diffusivity respectively), are measured in the wake of a circular cylinder. A high resolution Single Point Laser Induced Fluorescence (SPLIF) technique is used to investigate the small-scale scalar mixing. A comparison between mean and rms distributions of c and q across the wake, highlights the role of the Reynolds number and the Schmidt number in spreading out the scalar and accelerating the decay of its fluctuations. The streamwise evolution of the probability density function (pdf) of c is compared with that of q for which the molecular Prandtl number $Pr = \nu/k$ is about 0.7

(k is the thermal diffusivity). The pdfs indicate that, whereas q becomes homogeneous, c remains strongly inhomogeneous. The pdf of c retains a dependency on both x/d and Reynolds number, $Re (= U_0 d/\nu, U_0$ is the freestream velocity and d is the cylinder diameter). The skewness of c is larger than that of q along the wake centreline. The asymmetry of $p(c)$ indicates the persistence of the large scale motions in the far-wake. It is expected that the skewness of c becomes negative, as for q , at larger x/d . The flatness of c can be twice as large as that for q in the near-wake, then both converge to the Gaussian value of 3 downstream of $x/d \gg 150$.

1. INTRODUCTION

Temperature measurements in a plane-wake have received significant attention (Freymuth and Uberoi 1971, Antonia and Browne 1986, Mi and Antonia 1999). The measurement of q is relatively straightforward since the small scales to be resolved are of order $k^{3/4}/\langle e \rangle^{1/4}$ which is comparable to the Kolmogorov length scale $h = \nu^{3/4}/\langle e \rangle^{1/4}$ ($\langle e \rangle$ is the mean energy dissipation rate). When Sc is large, scalar scales smaller than h undergo a pure straining motion with a mean rate $g \gg \langle e \rangle/\nu$ (Batchelor, 1959). In this case, the smallest scalar scale or Batchelor scale is $h_B = (D/g)^{1/2} = hSc^{-1/2}$. The greater Sc , the more severe is the spatial resolution requirement. One of the widely used non-intrusive techniques for scalar measurements is the Planar LIF (PLIF). The PLIF technique, however, has both temporal and spatial limitations. The temporal ones are due to the slow camera frame rate and the long illumination time. The spatial ones are essentially dictated by the laser sheet thickness. These limitations make the PLIF adequate only for describing the large-scale topology and properties of the scalar field. The Single Point Laser Induces Fluorescence (SPLIF) allows continuous concentration signals to be measured at high sampling frequency so that scalar statistics converge rapidly. Furthermore, the spatial resolution can be considerably improved and, for specially chosen flow conditions, h_B can be adequately resolved (Prasad and Sreenivasan, 1990). Successful measurements of smoke concentration ($Sc \gg 1$) in air downstream of a grid have been carried out using SPLIF by Gad-el-Hak and Morton (1979). The present paper presents preliminary SPLIF results for the characteristics of a passive scalar (diluted fluorescein in water $Sc \gg 2000$) in the wake of a circular cylinder for $Re = 1180$. The evolution of the pdf of c , $p(c)$, along the centreline, in the intermediate and far-wake regions, is measured and compared with that of $p(q)$, reported by Sreenivasan (1981) for the same flow, x/d and Re .

2. EXPERIMENTAL SET-UP AND PROCEDURES

The experiments are conducted in a constant-head closed-circuit water tunnel (Figure 1). The 2 m long square test section (250×250 mm) is made of perspex. A circular cylinder (diameter $d = 6.4$ mm and aspect ratio of 40) is inserted in the working section (50 cm from the tunnel contraction exit) with both ends supported on the opposite walls of the test section. The Reynolds number is equal to 1180. Velocity measurements are made with a one-component Laser Doppler Velocimeter (LDV) system in a forward scatter mode.

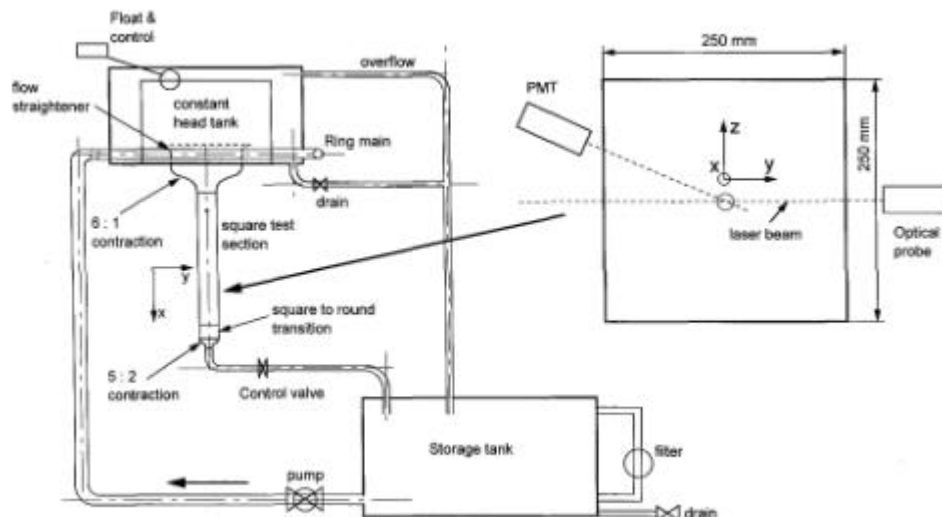


Figure 1: Schematic diagram of the water facilities. Inset is the optical set-up.

A SPLIF technique is used to measure the time series of the concentration fluctuations. The flow is seeded with diluted fluorescein at controlled flow-rates through a slit machined along the full cylinder length, at the forward stagnation line of the cylinder. Extra care is taken to avoid any perturbation of the flow at the injection. A multimode 200 mW argon-ion laser beam passes through a transmitter allowing two single mode incident laser beams (488 nm absorption wavelength for fluorescein) to be obtained, each with approximately the same power. The beams are expanded, collimated through achromatic lenses, then focused with a long focal convergent front lens ($f = 340$ mm) at the centre of the test section. The measuring volume for SPLIF, at the intersection between the beams, is an ellipsoid whose dimensions are estimated to be $20 \times 20 \times 100 \text{ } \mu\text{m}^3$. The fluorescence intensity in the measuring volume is collected through a system of close-up lenses, a pinhole of about 0.1 mm diameter, a narrow band optical filter (514 nm emission wavelength for fluorescein) and a photomultiplier tube (frequency response >100 kHz). The different elements of the receiving system are perfectly coupled and mounted in a forward scatter mode. For $Re = 1180$, the resolution is 20 times smaller than h . The photomultiplier tube output signal is sampled at a frequency of 5 kHz, digitized using a 12 bit board and stored for subsequent processing. For each measurement, the number of samples used is 2×10^6 . The technique is calibrated in a perspex tank with the same cross section dimensions as the test section where different fluorescein concentrations are carefully prepared. An identical optical paths are used for the calibration procedure. For each dye concentration, the fluorescence signal is collected at the centre of the tank. Noise is measured under the same conditions using clear water, and its mean value is subtracted from the mean value of the fluorescence signal. Photobleaching is minimised by stirring the fluorescein solutions before each measurement. The maximum mean concentration for which a linear relation exists between the output voltage and the dye mean concentration is about 10^{-6} mole/litre. The injection concentration is set to this value.

3. RESULTS

3.1 Mean and rms of concentration profiles

The distributions, with respect to y , of $\langle C \rangle / \langle C \rangle_{cl}$ ($\langle C \rangle_{cl}$ is the mean concentration on the centreline), $\langle DT \rangle / \langle DT \rangle_{cl}$ ($\langle DT \rangle_{cl}$ is the centreline mean temperature relative to the ambient temperature) and the normalised mean velocity defect $(U_0 - U) / (U_0 - U_{cl})$ (U_{cl} is the mean centreline velocity) are shown in Figure 2. The y -coordinate is normalized with d instead of the wake half-width d in order to emphasize the spread of the different profiles. For approximately the same values of Re and x/d , both concentration and temperature profiles are somewhat wider than the velocity profile. This is mainly due to the fact that the scalar is convected by the velocity vector and not only by its u -component. The temperature profile is wider than the concentration profile since temperature diffuses much faster which highlights the effect Sc has on the spread of the mean scalar field. This result is in good agreement with measurements by Balachandar et al. (1998) in the wake of a flat plate who found that d_t can be 1.5 to 2.5 times larger than d suggesting that molecular transport contributes significantly to the wake spreading. When Re is increased by a factor of about 2.5, both mean concentration and temperature profiles are significantly wider. The Reynolds number appears to have a more significant effect on the spread of the mean scalar field than Sc (Figure 3). As Re increases approximately by a factor of two, the wake half-width becomes 1.45 times wider for both concentration and temperature distributions.

The distributions across the wake of $\langle c^2 \rangle^{1/2} / \langle C \rangle_{cl}$ and $\langle q^2 \rangle^{1/2} / \langle DT \rangle_{cl}$ (Figure 4) show important differences between concentration and temperature. Firstly, at nearly the same Re and x/d , the distribution of $\langle q^2 \rangle^{1/2} / \langle DT \rangle_{cl}$ has a significantly wider spreading rate than that of $\langle c^2 \rangle^{1/2} / \langle C \rangle_{cl}$, underlining that the scalar fluctuations are more sensitive to molecular diffusion than the scalar mean values. This spreading out of both temperature and concentration distributions is accentuated and their maximum shift towards the edge of the wake when Re is increased. Secondly, the values of $\langle q^2 \rangle^{1/2} / \langle DT \rangle_{cl}$ are much smaller than those for $\langle c^2 \rangle^{1/2} / \langle C \rangle_{cl}$ across the entire wake. In particular, $\langle q^2 \rangle^{1/2} / \langle DT \rangle_{cl}$ is about three times less than $\langle c^2 \rangle^{1/2} / \langle C \rangle_{cl}$ on the wake centreline and persist towards the wake edge. The normalized concentration variance $\langle c^2 \rangle / \langle C \rangle^2$ ($\langle C \rangle$ is the scalar local mean concentration not shown here), measured at several x/d

locations on the centerline, appears to be approximately constant and is about 0.6 in contrast to $\langle q^2 \rangle / \langle DT \rangle^2$ ($\langle DT \rangle$ is the local mean temperature relative to the ambient temperature) which is about 0.06 for the same flow conditions indicating the importance of molecular diffusion to mixing. The use of such a weakly diffusive scalar as fluorescein delays the decay of the scalar variance and the establishment of homogeneous mixing.

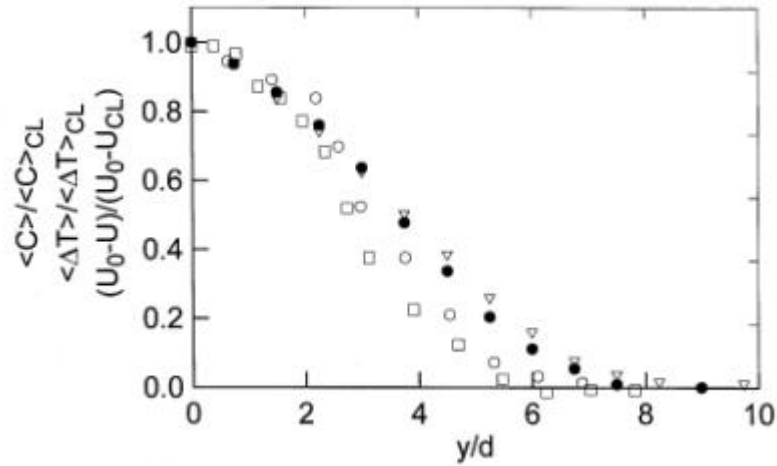


Figure 2: Normalised mean concentration, mean temperature and mean velocity defect across the wake. \square , $(U_0 - U) / (U_0 - U_{CL})$ $Re = 1180$ and $x = 225d$; \circ , $\langle C \rangle / \langle C \rangle_{CL}$ $Re = 1180$ and $x = 225d$; ∇ , $\langle DT \rangle / \langle DT \rangle_{CL}$ $Re = 1200$ and $x = 300d$; \bullet , $\langle DT \rangle / \langle DT \rangle_{CL}$ $Re = 1200$ and $x = 200d$ (Mi, 1999);

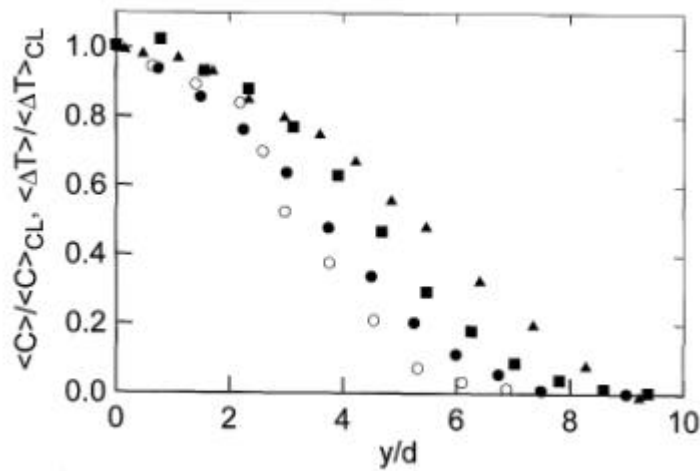


Figure 3: Normalised mean concentration and mean temperature across the wake. \circ , $Re = 1180$ and $x = 225d$; \blacksquare , $\langle C \rangle / \langle C \rangle_{CL}$ $Re = 2880$ and $x = 225d$; \bullet , $\langle DT \rangle / \langle DT \rangle_{CL}$ $Re = 1200$ and $x = 200d$ (Mi, 1999); π , $\langle DT \rangle / \langle DT \rangle_{CL}$ $Re = 2800$ and $x = 240d$ (Zhou, 1999).

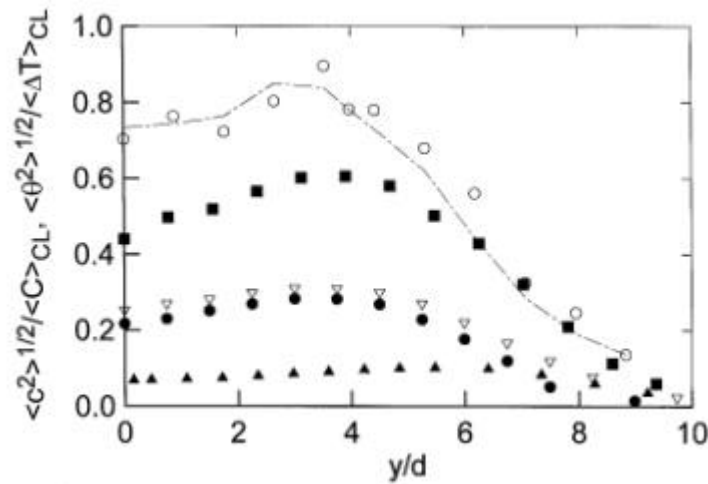


Figure 4: Normalised rms of concentration and temperature fluctuations. o, $\langle c^2 \rangle^{1/2} / \langle C \rangle_{CL}$ $Re = 1180$ and $x = 225d$; ■, $\langle c^2 \rangle^{1/2} / \langle C \rangle_{CL}$ $Re = 2880$ and $x = 225d$; ∇, $\langle q^2 \rangle^{1/2} / \langle DT \rangle_{CL}$ $Re = 1200$ and $x = 300d$; ●, $\langle q^2 \rangle^{1/2} / \langle DT \rangle_{CL}$ $Re = 1200$ and $x = 200d$ (Mi, 1999); π, $\langle q^2 \rangle^{1/2} / \langle DT \rangle_{CL}$ $Re = 2800$ and $x = 240d$ (Zhou, 1999).

3.2 Centreline probability density function

The evolution of $p(c)$ along the centreline is shown in Figure 5, together with that of the $p(q)$, the latter obtained by Sreenivasan (1981). Both $p(c)$ and $p(q)$ are highly non-Gaussian in the near and intermediate wakes, with a tendency towards Gaussianity as x/d increases. The pdf of q which is initially positively skewed, becomes Gaussian relatively quickly but then exhibits a slightly negative skewness downstream of $x/d \gg 78$. The pdf of c evolves more slowly and remains positively skewed until $x/d = 225$. This indicates a higher degree of inhomogeneity compared with q . This means there is still a significant amount of unmixed fluorescein dye in the flow whereas the concentration fluctuations have reached a statistically steady state. It is expected that the shape of $p(c)$ will continue to evolve with x/d but also to depend on Re . Sreenivasan (1981) and Mi and Antonia (1999) noted that the x -location at which the temperature skewness changes sign indicates the end of the Karman vortex street-dominated flow region, this location approaching that of the scalar source as Re increases.

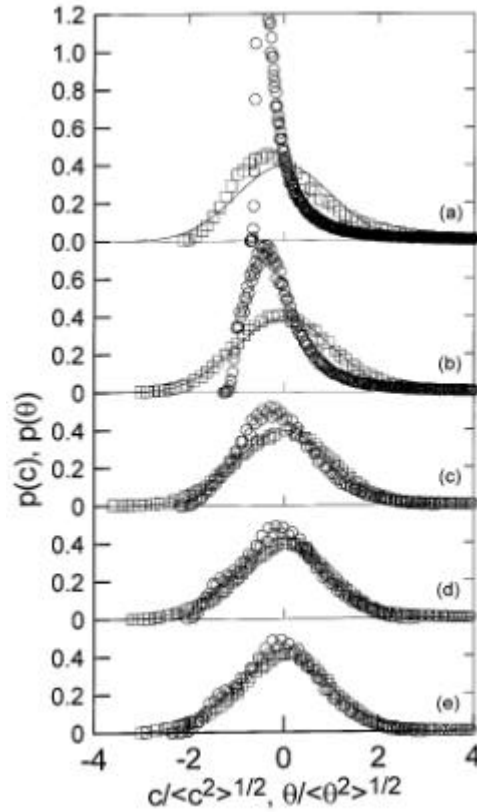


Figure 5: Pdfs of the concentration fluctuation c and temperature fluctuation q along the centreline: \circ , c ; \square , q . (a) $x/d = 16$; (b) 43; (c) 94; (d) 175 and (e) 225 for c and 300 for q . The solid line is the Gaussian distribution and $Re \gg 1160$.

The x -evolution of $S_c = \langle c^3 \rangle / \langle c^2 \rangle^{3/2}$ and $S_q = \langle q^3 \rangle / \langle q^2 \rangle^{3/2}$ is shown in Figure 6. In the near-wake, S_c and S_q have a similar trend and are positive as the pdfs are nonsymmetrical with a large peak at negative values of $c/\langle c^2 \rangle^{1/2}$ and $q/\langle q^2 \rangle^{1/2}$. The mixing of the scalar is initially dominated by the coherent large scale Karman structures which mainly entrain a large amount of clear (colder) fluid towards the centreline. As mixing takes place, the values of S_c and S_q decrease in the intermediate wake although $S_c > S_q$. At $x/d \gg 78$, where $p(q)$ reaches a point of symmetry S_q is zero whereas the concentration skewness is $S_c \gg 0.45$. In a region where S_q becomes, S_c continues to decrease at a slower rate than S_q and reaches the value $S_c = 0.2$ at $x = 225d$. The flatness $F_c = \langle c^4 \rangle / \langle c^2 \rangle^2$ is large in the near-wake (~ 10) before decreasing rapidly towards the Gaussian value of 3 (Figure 6). F_c and $F_q (= \langle q^4 \rangle / \langle q^2 \rangle^2)$ eventually tend to be equal at about $x/d \gg 150$. In contrast to F_q , which passes through a minimum of about 2.9 at $x/d \gg 78$ before increasing to the Gaussian value of 3, F_c has a monotonic evolution.

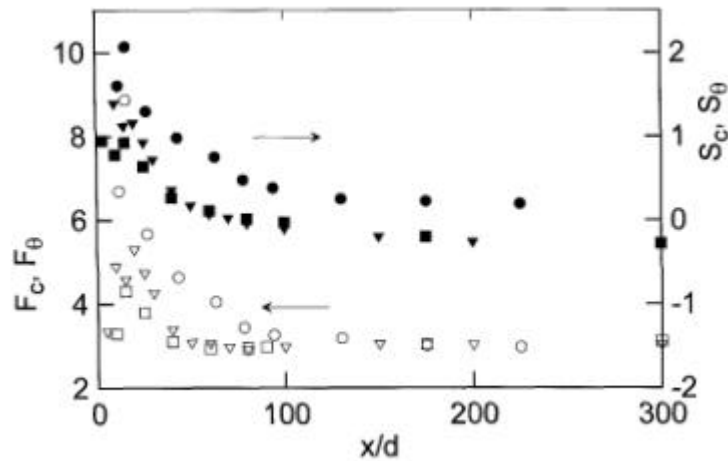


Figure 6: Variation along the centreline of the concentration skewness S_c and flatness factor F_c and the temperature skewness S_q and flatness factor F_q . •, S_c ; ○, S_q Mi (1999); ■, S_q Sreenivasan (1981); o, F_c ; ▽, F_q Mi (1999); □, F_q Sreenivasan (1981).

4. CONCLUSIONS

A single point LIF technique is used to measure the small-scale concentration characteristics of a high Schmidt number passive scalar in the wake of circular cylinder. The preliminary results illustrate the ability of the technique to produce adequately resolved and well converged concentration statistics. A comparison between mean and rms distributions of concentration (c) and temperature (q) across the wake, highlights the role of molecular diffusion in spreading out the scalar and accelerating the decay of its fluctuations. The mean concentration and temperature profiles across the wake confirm that the Reynolds number and to a lesser degree molecular diffusion play an important role in spreading out the mean scalar field. The rms profiles are clearly dependent on Sc and Re and the decay of the scalar variance is slower as Sc increases and Re decreases.

The streamwise evolutions of $p(c)$ and $p(q)$ underline the rapidity with which q becomes homogeneous relative to c . The skewness of c is larger than that for q along the wake centreline. In particular, the skewness of c remains positive while that of q becomes negative downstream of $x/d \gg 80$. The flatness of c is larger than that for q until about $x/d = 150$, then both reach the Gaussian value of 3. The important departure of $p(c)$ from Gaussianity indicates a persistent influence of the large-scale motions.

REFERENCES

- Antonia, R. A. and Browne, L. W. B. 1986. *J. Fluid Mech.*, **163**, 939-403.
- Balachandar, R., Chu, V. H., and Zhang, J. 1997. *J. Fluids Eng.*, **119**, 263-270.
- Batchelor, G. K. 1959. *J. Fluid Mech.*, **5**, 113-133.
- Freytmuth, P. and Uberoi, M. S. 1971. *Phys. Fluids*, **14**, 2574-2580.
- Gad-el-Hak, M. and Morton, J. B. 1979. *AIAA Journal*, **17**, 558-562.
- Mi, J. 1998. Private communication

Mi, J. and Antonia, R. A. 1999. *Int. Commun. Heat Mass Transfer*, **26**, 45-53.

Prasad, R. R. and Sreenivasan, K. R. 1990. *Phys. Fluids A*, **2**, 792-807.

Sreenivasan, K. R. 1981. *Phys. Fluids*, **24**, 1232-1234.